九州大学大学院総合理工学府報告
第 43 巻 第 1 号 8-21 頁 令和 3 年 9 月

Engineering Sciences Reports, Kyushu University
Vol. 43, No. 1, pp. 8-22, SEP, 2021

Dissociative Excitation of C_2H_2 by Collisions with Metastable Ne($^3P_{0,2}$) Atoms in a Flowing Afterglow

Masaharu TSUJI*1,2† Takahiro KOMATSU*3 Keiko UTO*1
Jun-Ichiro HAYASHI*1,2 and Takeshi TSUJI*4
†E-mail of corresponding author: tsuji@cm.kyushu-u.ac.jp

(Received May 24, 2021, accepted June 7, 2021)

CH($A^2\Delta$–$X^2\Pi_r$, $B^2\Sigma^-$–$X^2\Pi_r$, and $C^2\Sigma^+$–$X^2\Pi_r$) and C_2($d^3\Pi_g$–$a^3\Pi_u$, $C^1\Pi_g$–$A^1\Pi_u$, $e^3\Pi_g$–$a^3\Pi_u$, and $D^1\Sigma_u^+$–$X^1\Sigma_g^+$) emission systems have been observed by dissociative excitation of C_2H_2 by collisions with metastable Ne($^3P_2$:16.62 and $^3P_0$:16.72 eV) atoms in the flowing afterglow. The emission rate constants of CH(A,B,C) and C_2(d,C,e,D) were determined to be 1.72 and 10.2 × 10^{-13} cm^3 $molecule^{-1}$ s^{-1}, respectively. The major product was C_2(d), which occupied 78% of all emitting products. A comparison of the total emission rate constant, 1.19 × 10^{-12} cm^3 $molecule^{-1}$ s^{-1}, with reported Penning ionization rate constant indicated that branching ratios of Penning ionization and dissociative excitation in the Ne($^3P_{0,2}$)/C_2H_2 reaction are 99.3 and 0.7%, respectively. The nascent vibrational and rotational distributions of CH(A:v'=0–2,B:v'=0) and C_2(d:v'=0–6, C:v'=0–3, e:v'=0–6, D:v'=0–2) were determined and compared with statistical prior ones. The rotational distributions of major CH(A:v'=0–2) and C_2(d:v'=0–6) states were expressed by single Boltzmann temperatures of 2500–4200 K and 1300–2850 K, respectively. The reaction dynamics could not be explained by simple statistical models. It was concluded that rotationally excited CH* and vibrationally and rotationally excited C_2* are formed via *trans*-bent Rydberg (superexcited) C_2H_2** states with elongated C≡C bond and bending mode excitation.

Key words: *Dissociative excitation, Acetylene, Metastable Ne* atoms, Flowing afterglow, Energy transfer, Rovibrational distribution, Superexcited state, Trans-bent Rydberg state*

1. Introduction

Rate constants and product state distributions in reactions of rare gas active species with acetylene are pertinent to an understanding of the discharge chemistry in rare gas—acetylene mixtures used to produce amorphous hydrogenated carbon (a-C:H) films.[1,2] The reaction of C_2H_2 by collisions with metastable He(2^3S:19.82 eV) atoms has been studied by emission spectroscopy[3-5] and electron spectroscopy.[6,7] In the optical spectroscopic studies on the He(2^3S)/C_2H_2 reaction by Chang et al.[3] and Winicur et al.[4,5] using a flowing afterglow (FA) method, CH($A^2\Delta$–$X^2\Pi_r$, $B^2\Sigma^-$–$X^2\Pi_r$, and $C^2\Sigma^+$–$X^2\Pi_r$), C_2($d^3\Pi_g$–$a^3\Pi_u$, $C^1\Pi_g$–$A^1\Pi_u$, $e^3\Pi_g$–$a^3\Pi_u$, $D^1\Sigma_u^+$–$X^1\Sigma_g^+$, and $E^1\Sigma_g^+$–$A^1\Pi_u$), and H(Balmer series) emission systems were observed via dissociative excitation (1a).

$$He(2^3S) + C_2H_2 \rightarrow CH^*, C_2^*, H^* + \text{neutral products} + He \quad (1a)$$
$$\rightarrow CH, C_2, H + \text{neutral products} + He \quad (1b)$$
$$\rightarrow C_2H_2^+(\tilde{X}\,^2\Pi_u, \tilde{A}\,^2A_g, \tilde{B}\,^2\Sigma_u^+) + He + e^- \quad (1c)$$

Chang et al. measured relative intensities of each emission system.[3] Other competitive product channels are dissociation into non-emitting neutral products (1b) and Penning ionization leading to $C_2H_2^+(\tilde{X}, \tilde{A}, \tilde{B})$ (1c). A comparison between the total quenching cross section and excitation cross section indicated that dissociative excitation (1a) is a minor process, which occupies only 6% of total product channels.[3]

To our best knowledge, no optical spectroscopic study has been performed on the dissociative excitation of acetylene by collisions

*1 Institute for Materials Chemistry and Engineering, and Research and Education Center of Green Technology
*2 Department of Applied Science for Electronics and Materials
*3 Department of Applied Science for Electronics and Materials, Graduate Student
*4 Department of Materials Science, Shimane University

with metastable Ne($^3P_2$:16.62 eV and $^3P_0$:16.72 eV) atoms, although Penning ionization electron spectroscopic studies on the formation of the $C_2H_2^+(\tilde{X}\,^2\Pi_u)$ state have been carried out.[8,9] In the present study, UV and visible emission spectra resulting from the Ne($^3P_{0,2}$)/C_2H_2 reaction are measured in the Ne afterglow. The emission rate constants of each emitting species are determined by using a reference reaction method. Rovibrational distributions of excited species are determined from a computer simulation of observed spectra and compared with statistical prior ones. We discuss the reaction dynamics in terms of molecular structure and electronic structure of precursor superexcited C_2H_2** states. The energy-transfer process from Ne($^3P_{0,2}$) to C_2H_2 is compared with those from He(2^3S) to C_2H_2[3] and under vacuum ultraviolet (VUV) NeI photoexciation (16.85 eV) and synchrotron radiation (13.8–24.8 eV).[10,11]

2. Experimental

The FA apparatus used in this study was similar to that reported previously.[12,13] In brief, the metastable Ne($^3P_{0,2}$) atoms were generated by a microwave discharge of high purity Ne gas (purity >99.99%) operated at a Ne pressures of 0.1 Torr (1 Torr = 133.3 Pa). The effect of ionic active species was examined by using an ion-collector grid placed between the discharge section and the reaction zone. A small amount of C_2H_2 (purity 99.0%) was injected into the Ne afterglow from a nozzle placed 10 cm downstream from the center of the discharge. The partial pressure of C_2H_2 in the reaction zone was 1–6 mTorr.

Emission spectra were observed through a quartz window placed around a C_2H_2 gas inlet. A Spex 1.25 m monochromator equipped with a Hamamatsu Photonics R376 photomultiplier was used for spectral measurements in the 200–840 nm region. The relative sensitivity of the optical detection system was calibrated using standard D_2 and halogen lamps.

3. Results and discussion

3.1 Emission spectra and dissociative excitation processes

Figure 1 shows a typical emission spectrum obtained from the Ne afterglow reaction of C_2H_2. The CH($A^2\Delta$–$X^2\Pi_r$ and $B^2\Sigma^-$–$X^2\Pi_r$) and C_2($d^3\Pi_g$–$a^3\Pi_u$ and $C^1\Pi_g$–$A^1\Pi_u$) emission systems are identified in the 330–570 nm region. In addition, CH($C^2\Sigma^+$–$X^2\Pi_r$) and

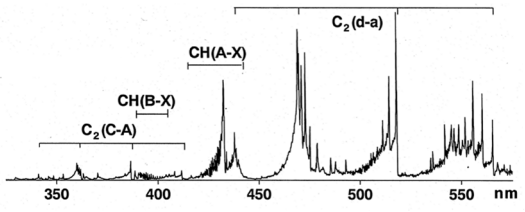

Fig. 1. Emission spectrum obtained from Ne afterglow reaction of C_2H_2.

C_2($e^3\Pi_g$–$a^3\Pi_u$ and $D^1\Sigma_u^+$–$X^1\Sigma_g^+$) emission systems are identified in the 315 nm and 210–300 nm region, respectively (not shown in Fig. 1). The contribution of ionic active species to the observed emissions was examined by an application of a suitable electrostatic potential to the ion-collector grid. By trapping Ne^+ and Ne_2^+ ions, no appreciable changes were observed in the intensities of CH(A–X, B–X, and C–X), and C_2(d–a, C–A, e–a, and D–X) emissions. These results indicate that ionic Ne species do not participate in the formation of these emitting excited species. The lack of Ne^+ and Ne_2^+ ions under the operating conditions was confirmed by monitoring the $CO^+(A^2\Pi_i$–$X^2\Sigma^+)$ and $N_2^+(B^2\Sigma_u^+$–$X^2\Sigma_g^+)$ emissions resulting from the Ne^+ + OCS and Ne_2^+ + N_2 charge-transfer reactions, respectively.[14,15] On the basis of above findings, Ne($^3P_{0,2}$) atoms are responsible for the production of these emitting excited states.

Figures 2a and 2b show energy-level diagrams of $C_2H_2^+$ and CH(A,B,C), and C_2(d,C,e,D) states from C_2H_2, where ionization potentials (IPs) and dissociation limits (DLs) for the formation of each excited state are shown. The first IP of the ground $C_2H_2^+(\tilde{X}^2\Pi_u)$ state is 11.403 eV.[16,17] Since this potential energy is lower than the energies of Ne($^3P_{0,2}$:11.62 and 11.72 eV), $C_2H_2^+$ ions can be formed by Penning ionization (2a).

$$\mathrm{Ne}(^3P_{0,2}) + C_2H_2$$
$$\rightarrow C_2H_2^+(\tilde{X}^2\Pi_u) + \mathrm{Ne} + e^- \quad (2a)$$
$$\rightarrow \mathrm{CH}^*, C_2^* + \text{neutral products} + \mathrm{Ne} \quad (2b)$$
$$\rightarrow C_2H, C_2, C + \text{neutral products} + \mathrm{Ne} \quad (2c)$$

Actually, the formation of $C_2H_2^+(\tilde{X}^2\Pi_u)$ has been observed by Penning ionization electron spectroscopy.[8,9] Dissociative excitation (2b) competes with Penning ionization (2a). In this case, the formation of CH(A,B,C) + CH occurs above the first IP of $C_2H_2^+(\tilde{X}\,^2\Pi_u$:$(1\pi_u)^{-1})$, as shown in Fig. 2. Therefore, CH(A,B,C) radicals are formed through superexcited C_2H_2** states, from which dissociative excitation (2b) and

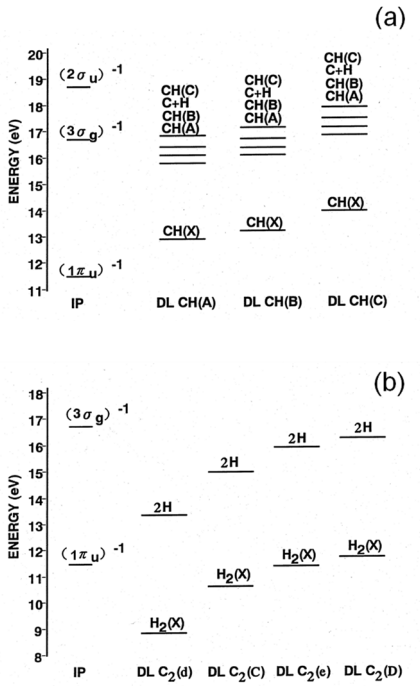

Fig. 2. Energy-level diagrams for the formation of CH(A,B,C) and C_2(d,C,e,D) states from C_2H_2. DL and IP mean dissociation limit and ionization potential, respectively. Thermochemical and spectroscopic data reported in Refs. 16–19 are used for the calculations.

autoionization leading to $C_2H_2^+(\tilde{X}^2\Pi_u)$ (2a) take place competitively. In addition to processes (2a) and (2b), dissociation into non-emitting neutral products (2c) can occur.

$C_2H_2^+$ and electrons are formed simultaneously in Penning ionization (2a). Since the IP of the ground $C_2H_2^+(\tilde{X}^2\Pi_u{:}(1\pi_u)^{-1})$ state is higher than the DLs for C_2(d,C,e) + H_2, the following two-body electron-ion recombination process may be responsible for the formation of C_2(d,C,e).

$$C_2H_2^+(\tilde{X}^2\Pi_u{:}(1\pi_u)^{-1})) + e^- \rightarrow C_2(d,C,e) + H_2. \quad (3)$$

To examine the contribution of above process, effects of the addition of a typical electron scavenger, SF_6 (purity 99.7%), was examined. SF_6 scavenges thermal electrons very rapidly:

$$e^- + SF_6 \rightarrow SF_6^- \quad (4)$$
$$k_4 = 2.2 \times 10^{-7}\ cm^3\ s^{-1}\ (Ref.\ 20).$$

Figures 3a and 3b show emission spectra observed after SF_6 addition and without SF_6 addition, respectively. No significant intensity changes are observed before and after SF_6

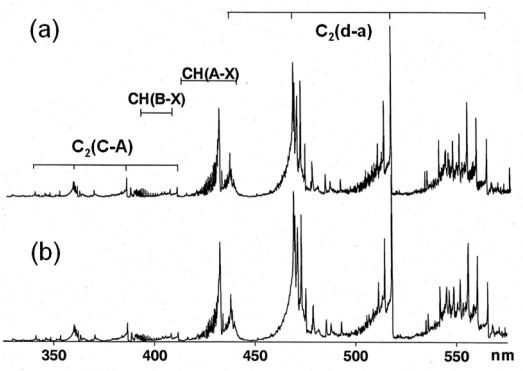

Fig. 3. Emission spectra obtained from Ne afterglow reaction of C_2H_2 (a) by the addition of a small amount of SF_6 and (b) without addition of SF_6.

addition. These results indicate that electron-ion recombination process (3) does not participate in the formation of C_2(d,C,e) in our conditions. Thus, it is concluded that C_2(d,C,e) are formed via dissociative excitation of C_2H_2 by collisions with Ne($^3P_{0,2}$).

3.2 Emission rate constants of CH* and C_2*

Possible excitation processes of CH(A,B,C) and C_2(d,C,e,D) by Ne($^3P_2$) atoms are as follows:

$$Ne(^3P_2) + C_2H_2$$
$$\rightarrow CH(A) + CH(X) + Ne + 3.78\ eV, \quad (5a)$$
$$\rightarrow CH(B) + CH(X) + Ne + 3.47\ eV, \quad (5b)$$
$$\rightarrow CH(C) + CH(X) + Ne + 2.71\ eV, \quad (5c)$$
$$\rightarrow C_2(d) + 2H + Ne + 3.29\ eV, \quad (6a)$$
$$\rightarrow C_2(d) + H_2 + Ne + 7.81\ eV, \quad (6b)$$
$$\rightarrow C_2(C) + 2H + Ne + 1.52\ eV, \quad (6c)$$
$$\rightarrow C_2(C) + H_2 + Ne + 6.04\ eV, \quad (6d)$$
$$\rightarrow C_2(e) + 2H + Ne + 0.76\ eV, \quad (6e)$$
$$\rightarrow C_2(e) + H_2 + Ne + 5.28\ eV, \quad (6f)$$
$$\rightarrow C_2(D) + 2H + Ne + 0.53\ eV, \quad (6g)$$
$$\rightarrow C_2(D) + H_2 + Ne + 5.05\ eV. \quad (6h)$$

For the reactions with higher-energy Ne($^3P_0$) atoms, 0.10 eV higher excess energies are released in the above reactions. Among above processes, highly exoergic reactions (6b), (6d), (6f), and (6h), in which H_2 molecules are formed, will be unfavorable, because large excess energies should be released as rovibrational energies and kinetic energies of products.

The emission rate constants for reactions (5)–(6) can be determined by using the reference reaction method if a reliable reference reaction exists. In the case of the He(2^3S) reaction, the following reference reaction can be used.

$$He(2^3S) + N_2 \rightarrow N_2^+(B^2\Sigma_u^+ : v' = 0,1) + He + e^- \quad (7)$$

$k_7 = 2.87 \times 10^{-11}$ cm^3 molecule^{-1} s^{-1} (Ref. 3).

To the best of our knowledge, no convenient reference reaction has been known for the Ne($^3P_{0,2}$) reaction. Therefore, we used here the Ne($^3P_{0,2}$)/NO reaction as a new reference reaction.

$$Ne(^3P_{0,2}) + NO \rightarrow NO(A^2\Sigma^+) + Ne \quad (8a)$$
$$\rightarrow NO^+ + Ne + e^- \quad (8b)$$

Since the formation of NO($A^2\Sigma^+$) from the Ne($^3P_{0,2}$)/NO reaction is highly exoergic (non-resonant by about 10 eV), initial formation of highly NO** states and radiative cascade from such high energy states may contribute to the formation of the low energy NO($A^2\Sigma^+$) state. Total deexcitation rate constants (or cross sections) of Ne($^3P_2$) and Ne($^3P_0$) by NO, (8a) + (8b), were reported to be 2.1×10^{-11} cm^3 molecule^{-1} s^{-1} (= 29 Å^2) and 2.0×10^{-10} cm^3 molecule^{-1} s^{-1} (= 27 Å^2), respectively,[21] whereas Penning ionization cross section for the Ne($^3P_{0,2}$)/NO reaction (8b) was measured to be 21.4 Å^2 at an effective temperature of 435 K.[22] Assuming that Penning ionization cross section of NO at thermal energy is the same as that at 435 K, and the difference between the total deexcitation rate constant and Penning ionization rate constant corresponds to energy-transfer reaction leading to NO(A), the rate constant of process (8a) is estimated to be 4.8×10^{-11} cm^3 molecule^{-1} s^{-1} by using an average total deexcitation constant for Ne($^3P_2$) and Ne($^3P_0$). An estimate of emission rate constants was carried out by comparing the integrated emission intensity of each band system with that of NO(A–X) in prepared mixtures of C_2H_2/NO. If there is no nonradiative decay and pumping from the observation region, the emission rate constants equal the formation ones.

Table 1. Emission rate constants (× 10^{-13} cm^3 molecule^{-1} s^{-1}) and branching ratios (%) of excited fragments produced from C_2H_2 by the Ne($^3P_{0,2}$) reaction, and branching ratios of excited fragments produced from C_2H_2 by the Ne($^3P_{0,2}$) reaction, NeI VUV photoexciation, and the He(2^3S) reaction.

	Ne($^3P_{0,2}$) 16.62 eV 16.72 eV		NeI 16.85 eV	He(2^3S) 19.82 eV
	This work		Ref. 10	Ref. 3
	k_{em}	Branching ratios (%)		
CH(A)	1.5	13	20	33
CH(B)	0.22	1.9	1.7	6
CH(C)	0.0046	0.04	1.3	<<1
sum	1.7246	15	23	<40
C_2(d)	9.3	78	47	33
C_2(C)	0.69	5.8	25	7
C_2(e)	0.22	1.9	3.9	7
C_2(D)	0.0069	0.06	1.7	<1
C_2(E)				<1
sum	10.2	86	78	<49
CH^+				3
Molecular and unassigned H-lines				8
				<1
total	11.9	101	101	100

Emission rate constants and their branching ratios thus obtained are given in Table 1. For comparison, reported branching ratios of each emitting species in NeI VUV photoexciation (16.85 eV)[10] and He(2^3S) reaction[3] are given. The total emission rate constant of C_2(d,C,e,D) by the Ne($^3P_{0,2}$) reaction, 10.2×10^{-13} cm^3 molecule^{-1} s^{-1}, is larger than that of CH(A,B,C), 1.72×10^{-13} cm^3 molecule^{-1} s^{-1}, by a factor of 5.9. This result implies that C_2* is more favorable excited products than CH* in the Ne($^3P_{0,2}$) reaction. Here, C_2* and CH* stand for C_2(d,C,e,D) and CH(A,B,C), respectively.

Among CH* and C_2* products, the CH(A) and C_2(d) states are major product states, which occupy 87% and 91% of total emission rate constants in CH* and C_2*, respectively. The total emission rate constants of CH(A,B,C) and C_2(d,C,e,D) in the Ne($^3P_{0,2}$)/C_2H_2 reaction is 1.19×10^{-12} cm^3 molecule^{-1} s^{-1}. This value is smaller than 1.01×10^{-11} cm^3 molecule^{-1} s^{-1} in the He(2^3S) reaction[3] by a factor of 8.5. The rate constant of Penning ionization (2a) has been measured to be $1.72 \pm 0.02 \times 10^{-10}$ cm^3 molecule^{-1} s^{-1}.[23] A comparison of this value with the k_{em}(total) value obtained in this study gives branching ratios of Penning ionization (2a) and dissociative excitation (2b) to be 99.3 and 0.69%, respectively. Based on this result, dissociative excitation (2b) is a minor exit channel in the Ne($^3P_{0,2}$)/C_2H_2 reaction.

The total branching ratio of C_2(d,C,e,D) in the Ne($^3P_{0,2}$) reaction (86%) is larger than those in the NeI VUV excitation (78%) and the

He(2^3S) reaction (49%) by factors of 1.1 and 1.8, respectively. Among the C_2(d,C,e,D) products, the selectivity of the C_2(d) state in the Ne($^3P_{0,2}$) reaction (91%) is larger than those in the NeI VUV excitation (60%) and He(2^3S) reaction (67%). Thus, the most outstanding feature in the Ne($^3P_{0,2}$) reaction is the preferential formation of the lowest C_2(d) state.

3.3 Rovibrational distributions of CH(A,B) and C_2(d,C,e,D) in the Ne($^3P_{0,2}$)/C_2H_2 reaction

Rovibrational distributions of CH(A,B) and C_2(d,C,e,D) in the Ne($^3P_{0,2}$)/C_2H_2 reaction were determined by a computer simulation of emission spectra because rotational lines were not fully resolved. The CH(C–X) emission was too weak to make a spectral simulation. Since the spin–orbit splitting is very small in the A, B, and X states of CH,[19] rotational levels of the CH(A,B,X) states are represented by the quantum number N. The band intensity (photons s^{-1}) of a transition from a (v', N') level to a (v'', N'') level is expressed as

$$I_{v'N'v''N''} \propto N_{v'N'} Re^2(\bar{r}_{v'v''}) q_{v'v''} \nu^3_{v'N'v''N''} S_{N'N''}/g_{N'} \qquad (9)$$

where $N_{v'N'}$ is the rotational population in a given vibrational level v', $Re(\bar{r}_{v'v''})$ the electronic transition moment, $q_{v'v''}$ the Franck-Condon factor, $\nu_{v'N'v''N''}$ the transition frequency, $S_{N'N''}$ the rotational line strength, and $g_{N'} = 2N' + 1$.[24] The electronic transition moment of CH(A–X) was assumed to be constant. The following Rydberg-Klein-Rees (RKR) Franck-Condon factors calculated by using molecular constants tabulated in Ref. 19 were employed for the simulation of the $\Delta v = 0$ sequence of CH(A–X): q_{00} = 0.9907, q_{11} = 0.9794, and q_{22} = 0.9793. RKR Franck-Condon factors were also calculated for the C_2(d–a, C–A, e–a, and D–X) transitions using reported molecular constants.[19] They are reported in a preceding paper.[25] The rotational line strength $S_{N'N''}$ was deduced from the formula given by Kovács.[26] A Gaussian slit function was convoluted into rotational lines to calculate the spectral envelope. For C_2 radicals in which spin–orbit splitting is large,[19] rotational quantum number is given by J instead of N.

In Figs. 4–9 are shown the observed and best fit spectra of the CH(A–X, B–X) bands and C_2(d–a, C–A, e–a, and D–X) bands obtained assuming single Boltzmann rotational distributions for each v' level. Vibrational distributions and rotational temperatures thus obtained are given in Tables 2 and 3. From the observed rovibrational distributions of CH(A,B) and C_2(d,C,e,D), we estimated the average

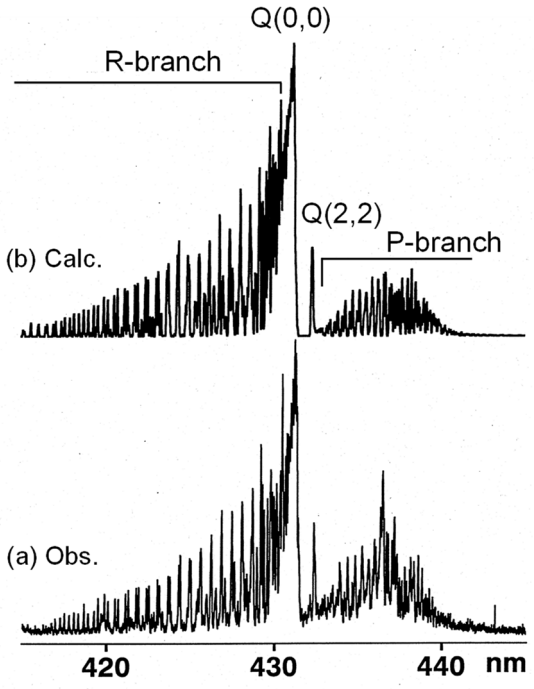

Fig. 4. (a) observed and (b) simulated emission spectra of CH($A^2\Delta$–$X^2\Pi_r$) band system in the Ne($^3P_{0,2}$)/C_2H_2 reaction.

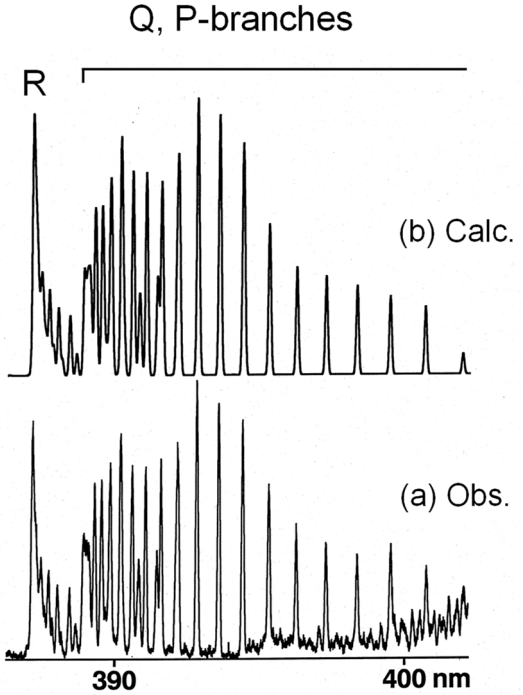

Fig. 5. (a) observed and (b) simulated emission spectra of (0,0) band of CH($B^2\Sigma^-$–$X^2\Pi_r$) band system in the Ne($^3P_{0,2}$)/C_2H_2 reaction.

vibrational and rotational energies of each CH* and C_2* state, denoted as $\langle E_v \rangle$ and $\langle E_r \rangle$, and the average yields of total available energy into these degrees of freedom, denoted as $\langle f_v \rangle$ and $\langle f_r \rangle$, respectively. Symbol $\langle f_t \rangle$ represents the average yield of total available energy into the relative translational energy. The $\langle E_v \rangle$, $\langle E_r \rangle$, $\langle f_v \rangle$, $\langle f_r \rangle$, and $\langle f_t \rangle$ values obtained for CH* and C_2* are summarized in Tables 4 and 5, respectively.

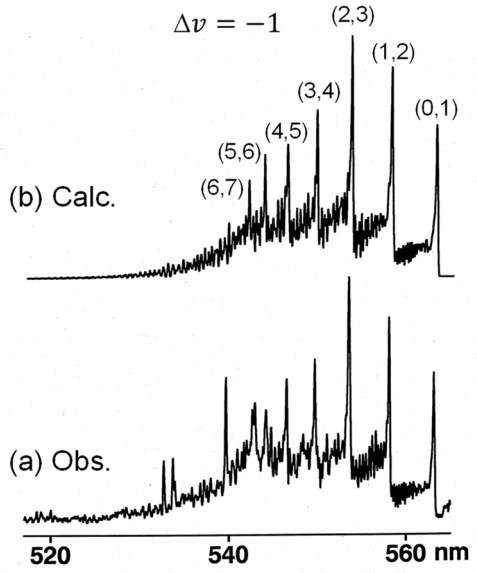

Fig. 6. (a) observed and (b) simulated emission spectra of the $C_2(d^3\Pi_g–a^3\Pi_u)$ band system in the $Ne(^3P_{0,2})/C_2H_2$ reaction.

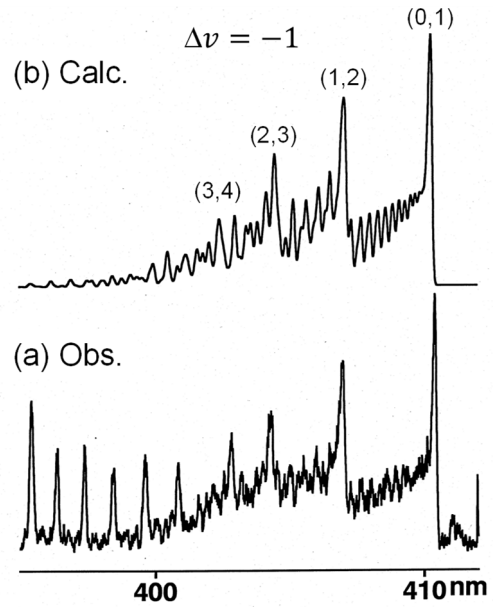

Fig. 7. (a) observed and (b) simulated emission spectra of the $C_2(C^1\Pi_g–A^1\Pi_u)$ band system in the $Ne(^3P_{0,2})/C_2H_2$ reaction.

According to our optical spectroscopic study on the formation of CH(A,B) from the $He(2^3S)/CH_4$ reaction,[27] the rovibrational distributions of CH(A,B) in the FA experiment was identical to those in the low-pressure beam experiment. Therefore, it was concluded that the vibrational and rotational relaxation of

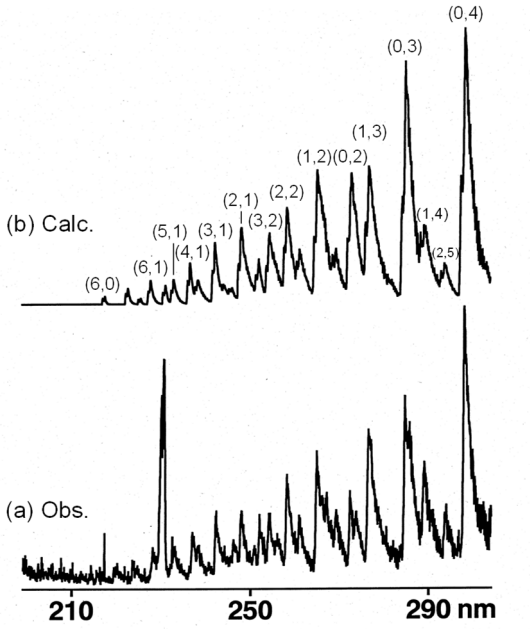

Fig. 8. (a) observed and (b) simulated emission spectra of the $C_2(e^3\Pi_g–a^3\Pi_u)$ band system in the $Ne(^3P_{0,2})/C_2H_2$ reaction.

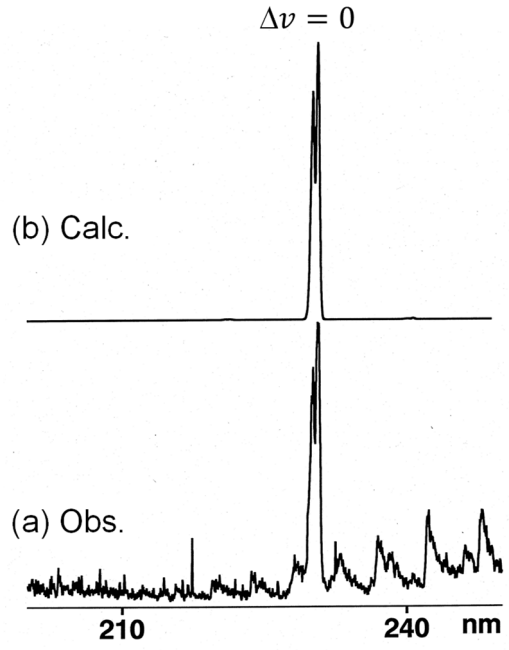

Fig. 9. (a) observed and (b) simulated emission spectra of the $C_2(D^1\Sigma_u^+–X^1\Sigma_g^+)$ band system in the $Ne(^3P_{0,2})/C_2H_2$ reaction.

CH(A,B) by collisions with the buffer He gas was insignificant in the FA experiment. In the present Ne FA experiment, operating pressure (0.1 Torr) was lower than that that in the He FA (0.5–1.0 Torr). It is therefore reasonable to assume that the vibrational and rotational relaxation of CH(A,B) by collisions with the buffer Ne gas is also insignificant. Radiative lifetimes of C_2(d,C,e,D) states are relatively short : 97–104 ns for d(v'=0–2), 28–31 ns for C(v'=0–2), 254–340 ns for e(v'=0–2), and 14–18 ns for D(v'=0–2).[28] Therefore, the vibrational and rotational relaxation of C_2(d,C,e,D) by collisions with the buffer Ne gas will be also insignificant under operating conditions.

The following tendencies are found for the observed rovibrational distributions of CH* and C_2*.

(A) Formation of CH*

(1) The vibrational population of CH(A:v'=0–2) decreases with increasing v'. The rotational temperature of CH(A) decreases from 4200 K to 2500 K with increasing v' from 0 to 2. The rotational temperature of CH(B: v'=0) is 2500 K, which is lower than that of CH(A:v'=0).

(2) The $<E_v>$ and $<E_r>$ values of CH(A,B) are small (0–0.32 eV). The $<f_r>$ value for CH(A), 8.60%, is larger than the $<f_v>$ value, 3.46%, by a factor of 2.5. The $<f_v>$ value for CH(B) is zero due to predissociation of vibrational excited states,[29,30] The $<f_r>$ value for CH(B) is 6.21%, which is smaller than that for CH(A) by 28%

(3) Results shown in (1) and (2) imply that more excess energies are deposited into rotational energies than into vibrational energies for the formation of CH*. It is therefore reasonable to assume that precursor superexcited C_2H_2** states have non-linear structures.

(4) The $<f_v>$ + $<f_r>$ value for CH(A) is 12.1%, whereas that for CH(B) is 6.2%. These results suggest that almost all of the total available energies (88% for CH(A) and 94% for CH(B)) are channeled into rovibrational energies of CH(X) and relative translational energy of CH(A or B) + CH(X) products.

Table 2. Rovibrational distributions of CH(A,B) produced from the $Ne(^3P_{0,2})/C_2H_2$ reaction. $N_{v'}$ and $P^o_{v'}$ represent observed and calculated prior vibrational distributions, respectively. $P^o_{v'}$ were calculated assuming two-body and three-body dissociation processes.

Emitting species		$N_{v'}$	$P^o_{v'}$ Two-body	$P^o_{v'}$ Three-body	T_r/ K
CH(A)	v'=0	100	100	100	4200
	v'=1	45	72	63	3000
	v'=2	7	51	39	2500
CH(B)	v'=0	100			2500

Table 4. Average vibrational and rotational energies (eV) deposited into CH (A,B) and average fractions of vibrational and rotational energies (%) deposited into CH(A,B) in the $Ne(^3P_2)/C_2H_2$ reaction.

CH(A)	$<E_v>$	0.13
	$<E_r>$	0.32
	$<f_v>$	3.46
	$<f_r>$	8.60
	$<f_v>$ +$<f_r>$	12.06
CH(B)	$<E_v>$	0.0
	$<E_r>$	0.22
	$<f_v>$	0
	$<f_r>$	6.21
	$<f_v>$ +$<f_r>$	6.21

Table 3. Rovibrational distributions of C_2(d,C,e,D) produced from the $Ne(^3P_{0,2})/C_2H_2$ reaction.

	C_2(d)			C_2(C)			C_2(e)			C_2(D)		
v'	$N_{v'}$	$P^o_{v'}$	T_r/ K	$N_{v'}$	$P^o_{v'}$	T_r/ K	$N_{v'}$	$P^o_{v'}$	T_r/ K	$N_{v'}$	$P^o_{v'}$	T_r/ K
0	100	100	2850	100	100	2000	100	100	1000	83	100	800
1	95	81	2750	60	63	1500	60	57	1200	100	20	800
2	88	66	2300	50	36	1000	27	30	700	43	0	450
3	55	52	2000	40	19	1000	12	14	400			
4	63	41	1700				7	5	300			
5	58	32	1500				3	1	300			
6	50	25	1300				1	0	300			

Table 5. Average vibrational and rotational energies (eV) deposited into C_2(d,C,e,D) and average fractions of vibrational, rotational, and translational energies (%) deposited into C_2(d,C,e,D) in the Ne($^3P_2$)/C_2H_2 reaction.

C_2(d)	$<E_v>$	0.53
	$<E_r>$	0.19
	$<f_v>$	16.01
	$<f_r>$	5.75
	$<f_v>+<f_r>$	21.76
	$<f_t>$	78.24
C_2(C)	$<E_v>$	0.24
	$<E_r>$	0.13
	$<f_v>$	16.63
	$<f_r>$	8.60
	$<f_v>+<f_r>$	25.23
	$<f_t>$	74.77
C_2(e)	$<E_v>$	0.12
	$<E_r>$	0.082
	$<f_v>$	15.59
	$<f_r>$	10.78
	$<f_v>+<f_r>$	26.37
	$<f_t>$	73.63
C_2(D)	$<E_v>$	0.18
	$<E_r>$	0.063
	$<f_v>$	34.38
	$<f_r>$	11.86
	$<f_v>+<f_r>$	46.24
	$<f_t>$	53.76

(B) Formation of C_2*

(1) Vibrational populations of C_2(d,C,e) decrease with increasing v', except for C_2(d: v' =4, 5), whereas vibrational population has a peak at v'=1 for C_2(D). Vibrational excitation is suppressed with increasing the formation energy of C_2 state from d to C and e states. In general, rotational temperatures of C_2(d,C,e,D) decrease with increasing v'. They decrease with increasing the formation energy of C_2 state from 2850 K to 300 K: C_2(d) > C_2(c) > C_2(e) > C_2(D).

(2) The $<E_v>$ value decreases with increasing the formation energy of C_2(d,C,e) from 0.53 eV to 0.12 eV, and increases to 0.18 eV for C_2(D). The $<E_r>$ value also decreases with increasing the formation energy of C_2(d,C,e,D) from 0.19 eV to 0.063 eV.

(3) The $<f_v>$ values for C_2(d,C,e,D) + 2H are larger than the $<f_r>$ values by factors of 1.4–2.9. This suggests that deposition of excess energy into vibration is more favorable than that into rotation for the formation of C_2*. It is therefore reasonable to assume that a significant change in C≡C bond length occurs in precursor C_2H_2** superexcited states after excitation.

(4) The $<f_v>$ + $<f_r>$ values for C_2(d,C,e,D) + 2H are 22, 25, 26, and 46%, respectively. Based on these results, most of available energies (74–78%) are deposited as relative translational energies for the formation of the low lying C_2(d,C,e) states, whereas about a half (54%) of the available energy is channeled into the relative translational energies for the formation of the highest C_2(D) state.

3.4 The reaction dynamics of the Ne($^3P_{0,2}$)/C_2H_2 reaction

3.4.1 Statistical models

The formation dynamics of CH(A,B) and C_2(d,C,e,D) from the Ne($^3P_{0,2}$)/C_2H_2 reaction is discussed assuming two-body and three-body dissociation mechanisms, which have been used in the formation of CH($A^2\Delta$) from Ar($^3P_2$)/CH_3 and Ar($^3P_2$)/C_2H_5,[31,32] OH($A^2\Sigma^+$) from Ar($^3P_{0,2}$)/H_2O,[33] and NH($A^3\Pi_i$) from Ar($^3P_{0,2}$)/NH_3.[34]

(a) Two-body dissociation process through resonant excitation transfer

$$\begin{aligned} &Ne^* + C_2H_2 \rightarrow C_2H_2^{**} + Ne \\ &C_2H_2^{**} \rightarrow CH(A,B) + CH(X) \end{aligned} \quad (10)$$

(b) Three-body dissociation process through resonant excitation transfer

$$\begin{aligned} &Ne^* + C_2H_2 \rightarrow NeC_2H_2^{**} \\ &NeC_2H_2^{**} \rightarrow CH(A,B) + CH(X) + Ne \end{aligned} \quad (11)$$

(c) Three-body dissociation process through resonant excitation transfer

$$\begin{aligned} &Ne^* + C_2H_2 \rightarrow C_2H_2^{**} + Ne \\ &C_2H_2^{**} \rightarrow C_2(d,C,e,D) + 2H \end{aligned} \quad (12)$$

In processes (10) and (12), energy is resonantly transferred from Ne* to C_2H_2, and then C_2H_2** dissociates into CH(A,B) + CH and C_2(d,C,e,D) + 2H. In process (11), CH(A,B) are produced through three-body dissociation of NeC_2H_2** complex.

Statistical vibrational and rotational

distributions were calculated for the above three processes. According to a simple statistical theory,[35-37] the probability of forming a CH*(v', N') rovibrational level and a CH*(v') vibrational level through processes (a) and (b) is, respectively, expressed by

$$P^o_{v'N'} \propto (2N'+1)\Sigma_{v_{CH(X)}}(E_{tot} - E_{v_{CH^*}} - E_{v_{CH(X)}} - E_{r_{CH^*}})^{3/2} \quad (13a)$$

$$P^o_{v'} \propto \Sigma_{v_{CH(X)}}(E_{tot} - E_{v_{CH^*}} - E_{v_{CH(X)}})^{5/2} \quad (13b)$$

$$P^o_{v'N'} \propto (2N'+1)\Sigma_{v_{CH(X)}}(E_{tot} - E_{v_{CH^*}} - E_{v_{CH(X)}} - E_{r_{CH^*}})^{3} \quad (14a)$$

$$P^o_{v'} \propto \Sigma_{v_{CH(X)}}(E_{tot} - E_{v_{CH^*}} - E_{v_{CH(X)}})^{4}. \quad (14b)$$

On the other hand, that of process (c) is given by

$$P^o_{J'N'} \propto (2J'+1)(E_{tot} - E_{v_{C_2*}} - E_{r_{C_2*}})^2 \quad (15a)$$

$$P^o_{v'} \propto \left(E_{tot} - E_{v_{C_2*}}\right)^3. \quad (15b)$$

The prior vibrational distribution of CH(A: v'=0–2) and rotational distributions of CH(A: v'=0–2,B: v'=0) calculated for processes (a) and (b) are compared with the observed ones in Table 2 and Figs. 10a and 10c–10e. The prior vibrational distribution of CH(A: v'=0–2) and rotational distributions of CH(A: v' =0–2, B: v' =0) predict higher vibrational and rotational excitation than the observed ones for both two-body and three-body dissociation models.

The deviation from prior rotational distribution can often be expressed in the form of surprisal,[37]

$$I_v = -\ln[P(v)/P^o(v)], = \lambda_0 + \lambda_v f_v \quad (16)$$

$$I_R = -\ln[P(v,N)/P^o(v,N)] = \theta_0 + \theta_R g_N \quad (17)$$

where $f_v = E_v/E_{tot}$, $g_N = E_N/(E_{tot}-E_v)$, $P(v) = N_{v'}$ and $P(v,N) = N_{v'N'}$.

Figure A1 in Appendix shows vibrational and rotational surprisal plots of CH(A: v' =0–2, B: v'=0). When the two-body and three-body dissociation models are used for $P^o_{v'N'}$ and $P^o_{v'}$, good linear relationships are found in the surprisal plots of CH(A: v'=0–2,B: v'=0). These results imply that an exponential gap behavior is present between the experimental and

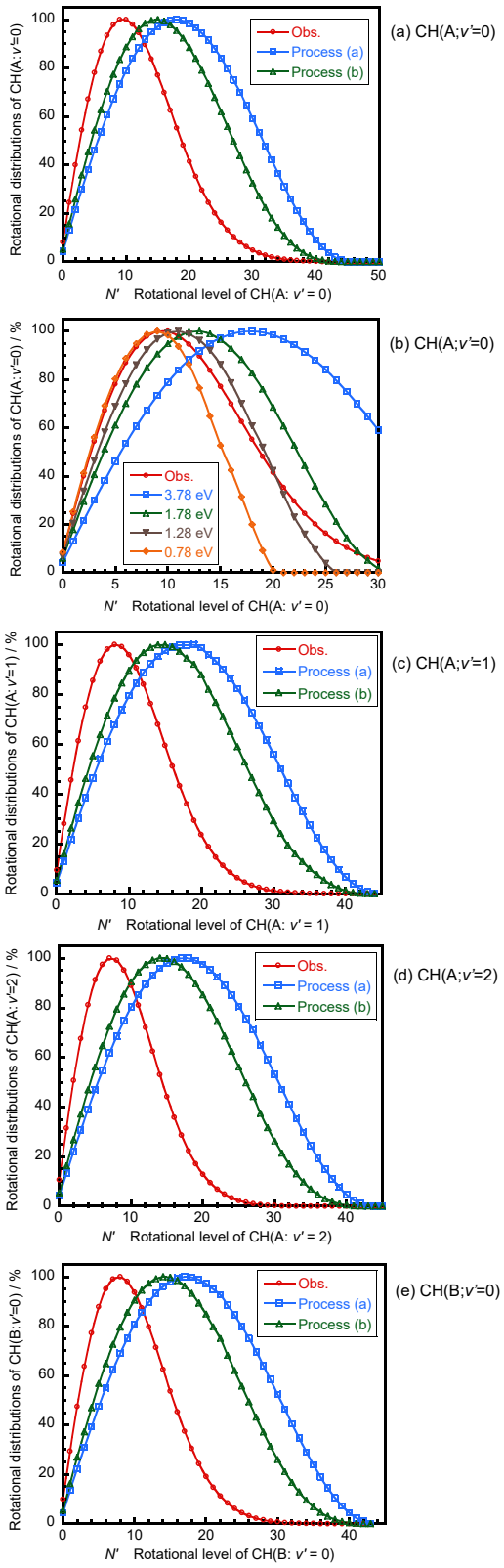

Fig. 10. Observed and two-body and three-body prior rotational distributions of CH(A: v'=0–2, B: v'=0) in the $Ne(^3P_{0,2})/C_2H_2$ reaction. In (b), an excess energy was varied from 3.78 eV to 0.78 eV in process (a).

statistical distributions. From slopes of each surprisal plot, large positive surprisal parameters are obtained in all cases (Table A1 in Appendix) because observed vibrational and rotational distributions are significantly lower than those expected from two-body and three-body prior distributions. The rotational surprisal parameter of CH(A: v'=0–2) increases with increasing v', suggesting that the deviation from prior distributions increases with increasing v'.

To find out how much lowing the total available energy matches the observed distribution, prior rotational distributions of CH(A:v'=0) are calculated by reducing the total available energy from 3.78 eV to 0.78 eV as a typical case (Fig. 10b). Then, a reasonable fit of the peak position is obtained at the lowest available energy of 0.78 eV, indicating that a large excess energy of 3.0 eV must be deposited as relative translation energy of Ne($^3P_{0,2}$)–C_2H_2 before the formation of precursor C_2H_2** states according to this model.

The prior vibrational and rotational distributions of C_2(d,C,e,D) calculated for three-body process (c) are compared with the observed ones in Table 3 and Figs. 11 and 12. The observed vibrational distributions of C_2* are higher than prior ones except for the C_2(e) state, for which a reasonable agreement between the observed and prior distributions is found for the v'=0–3 levels. These results are opposite to those of CH(A), for which the observed vibrational distribution is lower than the prior one. On the other hand, the observed rotational distributions of C_2(d,C,e,D) are lower than prior ones, as in the case of CH(A,B). To find out how much lowing the total available energy is required to reproduce the observed distribution, prior rotational distributions of C_2(d: v'=0) are calculated by reducing the total available energy from 3.29 eV to 0.79 eV as a typical example (Fig. 11c). Then, the observed peak of the rotational distribution can be reproduced when the total available energy is reduced by 2.5 eV. In such a case, non-resonant excitation transfer with a significant momentum transfer is required. However, the possibility of such a non-resonant energy transfer to 2.5 eV lower C_2H_2** states will be small, because a significant energy transfer to relative translational energy of Ne($^3P_{0,2}$)–C_2H_2 is required due to highly repulsive interactions between Ne($^3P_{0,2}$) and C_2H_2 in the entrance channel.

Figures A2 and A3 in Appendix show

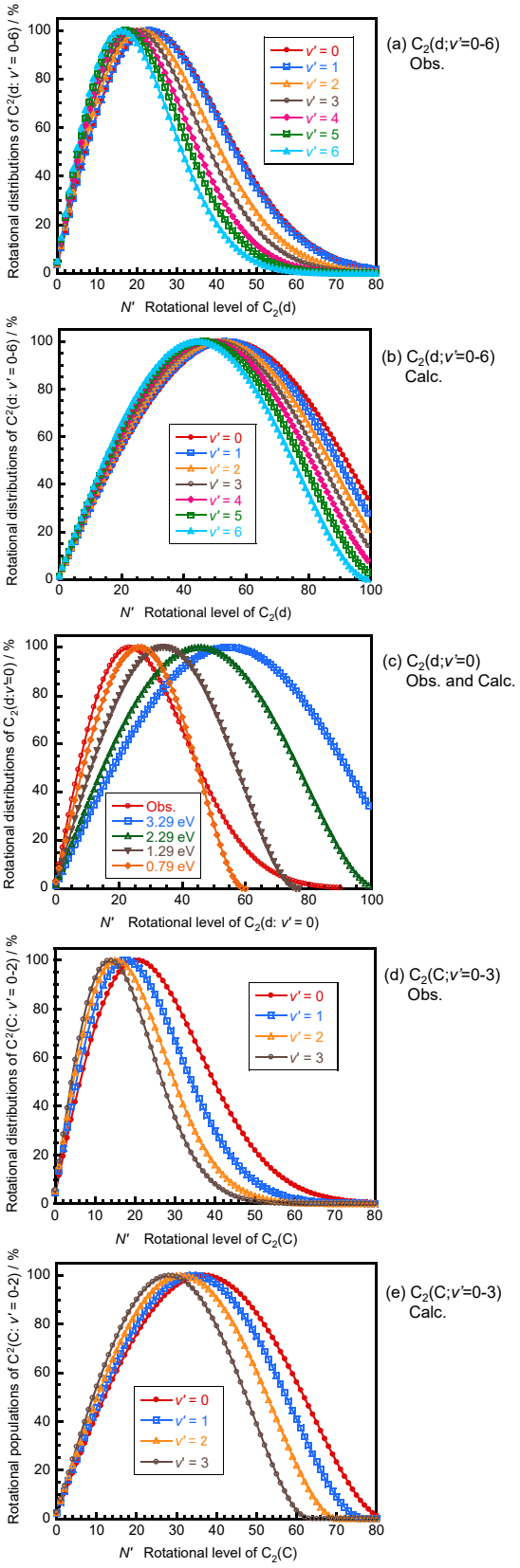

Fig. 11. Observed and three-body prior rotational distributions of C_2(d: v'=0–6, C: v'=0–3) in the Ne($^3P_{0,2}$)/C_2H_2 reaction. In (c), an excess energy was varied from 3.29 eV to 0.79 eV.

vibrational and rotational surprisal plots of C_2(d,C,e,D). Vibrational and rotational surprisal parameters obtained from slopes are given in Table A1 in Appendix. Vibrational surprisal parameters of C_2(d,C,D) are negative, because the observed vibrational distributions are higher than prior ones. On the contrary, rotational surprisal parameters of C_2(d,C,e,D) are positive except for C_2(e: v' =6) and C_2(D: v'=2), because the observed rotational distributions are lower than prior ones.

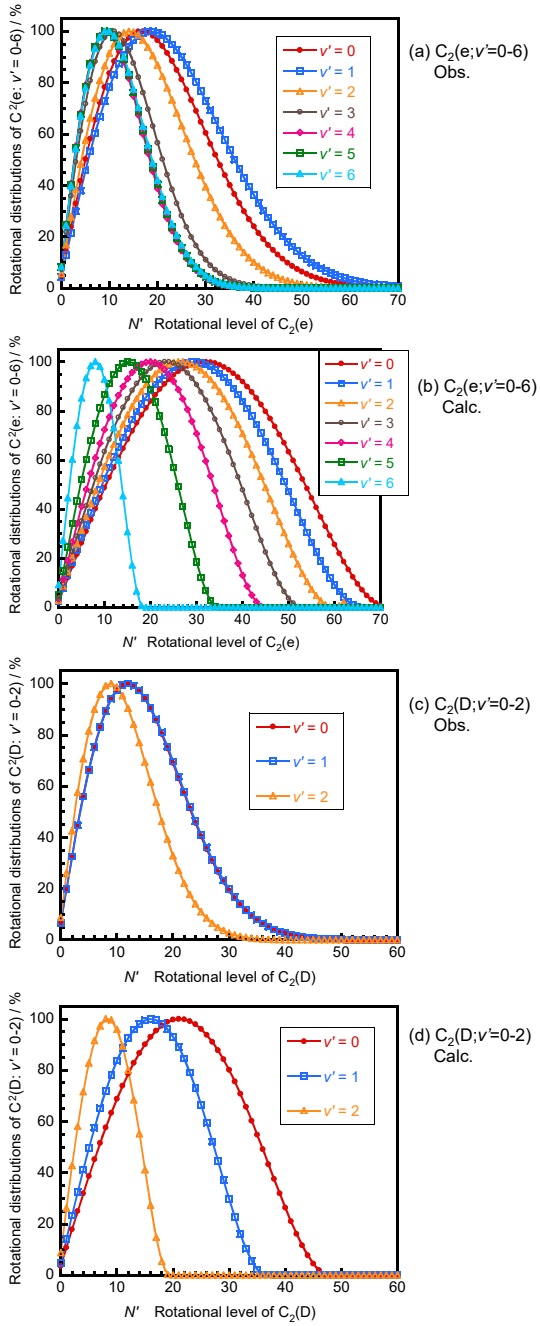

Fig. 12. Observed and three-body prior rotational distributions of C_2(e: v' =0–6, D: v'=0–2) in the Ne($^3P_{0,2}$)/C_2H_2 reaction.

3.4.2 Effects of molecular structure and electronic structure of superexcited C_2H_2** states on the reaction dynamics

A comparison between the observed and statistical prior distributions of CH* and C_2* suggests that excess energies are not partitioned in an entirely statistical manner between all degrees of freedom of the CH(A,B) + CH(X) and C_2(d,C,e,D) + 2H products. Therefore, CH* and C_2* are not formed through long-lived precursor states, where excess energies are distributed into all degrees of freedom statistically. Based on the above facts, the reaction dynamics for the formation of CH* and C_2* is not governed by statistical models.

Hereinafter, we discuss the reaction dynamics in terms of molecular structure and electronic structure of precursor C_2H_2** states in the Ne($^3P_{0,2}$)/C_2H_2 reaction. The ground state acetylene molecule has the electronic configuration,

$$(1\sigma_g)^2(1\sigma_u)^2(2\sigma_g)^2(2\sigma_u)^2(3\sigma_g)^2(1\pi_u)^4 (1\pi_g)^0(3\sigma_u)^0: {}^1\Sigma^+. \quad (18)$$

Removal of two outermost orbitals are possible in the energy of Ne($^3P_{0,2}$) studied here. The IPs of the $(1\pi_u)^{-1}$ ground $\tilde{X}^2\Pi_u$ state and the first excited $(3\sigma_g)^{-1}$ $\tilde{A}^2A_g$ state of $C_2H_2^+$ are 11.403 and 16.297 eV, respectively.[16,17]

Based on our optical spectroscopic studies on the dissociative excitation of simple polyatomic molecules by rare gas metastable He(2^3S) and Rg($^3P_{0,2}$) atoms,[38-42] spin-conservation rule generally holds during the reaction. Therefore, high-energy C_2H_2** superexcited triplet states around 11.62–11.72 eV are expected to be formed after near-resonant energy transfer, because the ground state of C_2H_2 is singlet. Although no information on such high-energy triplet states near the second $(3\sigma_g)^{-1}$ ionic state of $C_2H_2^+$ has been obtained, high-energy singlet states near the $(3\sigma_g)^{-1}$ $\tilde{A}^2A_g$ ionic state of $C_2H_2^+$ have been studied under VUV photoexcitation.[11] Two $np\pi^* \leftarrow 3\sigma_g$ Rydberg series, A and B, have been observed. Rydberg series A has a convergence limit of 16.611 eV (74.642 nm), which is 2530 cm^{-1} above the threshold of $C_2H_2^+(\tilde{A}^2A_g)$ and series B has a convergence limit of 16.358 eV (75.795 nm), which is 492 cm^{-1} above the threshold of $C_2H_2^+(\tilde{A}^2A_g)$. In the above two Rydberg series A and B, long progressions of ν_2 (symmetric C≡C stretching) mode and ν_4 (symmetric bending) mode peaks were observed, suggesting that the superexcited states formed in this wavelength region have elongated CC bond and non-linear

structure.

In the $Ne(^3P_{0,2})/C_2H_2$ reaction, it is likely that C_2H_2 molecules are initially excited into unknown near-resonant triplet $np\pi^* \leftarrow 3\sigma_g$ Rydberg states converging to the $\tilde{A}\,^2A_g$ state of $C_2H_2^+$. Molecular structures of these Rydberg states are expected to have the same character as that of the $\tilde{A}\,^2A_g$ state of $C_2H_2^+$. Since the $\tilde{A}\,^2A_g$ state of $C_2H_2^+$ is formed by removal of bonding $3\sigma_g$ orbital, C≡C bond is elongated after ionization. It should be noted that the $\tilde{A}\,^2A_g$ state of $C_2H_2^+$ has a *trans*-bent structure, and two CCH bending modes are accessible by a vertical transition.[11] It is expected that superexcited triplet Rydberg states have also a *trans*-bent structure with a loosened CC bond and excited CCH bending vibration. Decomposition of *trans*-bent superexcited triplet states with an expanded C≡C internuclear distance and excited bending vibrational mode results in high rotational excitation of CH* and high vibrational and rotational excitation of C_2* observed in this study.

$Ne(^3P_{0,2})$ + linear C_2H_2
→ *trans*-bent C_2H_2** + Ne　(19a)
trans-bent C_2H_2**
→ CH*(high N') + CH　(19b)
→ C_2*(high v' and J') + 2H.　(19c).

4. Summary and Conclusion

Dissociative excitation of C_2H_2 by collisions with metastable $Ne(^3P_{0,2})$ atoms has been studied by observing CH* and C_2* emissions in the Ne FA. The effect of SF_6 addition into the Ne afterglow indicated that secondary $C_2H_2^+/e^-$ electron-ion recombination reaction does not participate in the formation of C_2(d,C,e) and they are formed through the primary $Ne(^3P_{0,2})/C_2H_2$ reactions. The emission rate constants of CH(A,B) and C_2(d,C,e,D) were determined by using a reference reaction method. The major product was C_2(d), which occupied 78% of all emitting products. This value was larger than reported values of 47% by NeI photoionization (16.85 eV) and 33% by $He(2^3S$:19.82 eV) collisions. The total emission rate constant of CH* and C_2* in the $Ne(^3P_{0,2})/C_2H_2$ reaction was smaller than that in the $He(2^3S)/C_2H_2$ reaction by a factor of 8.5.

In this study, dissociative excitation (2b) was examined. A comparison of the total emission rate constant, 1.19×10^{-12} cm^3 $molecule^{-1}$ s^{-1}, with reported Penning ionization rate constant indicated that branching ratios of Penning ionization and dissociative excitation in the $Ne(^3P_{0,2})/C_2H_2$ reaction were 99.3 and 0.7%, respectively. Actually, beside Penning ionization (2a) and dissociative excitation (2b), dissociation into non-emitting neutral products (2c) can occur. If the total quenching rate constant of $Ne(^3P_{0,2})$ by C_2H_2, $k_Q = k_{2a} + k_{2b} + k_{2c}$, is known, we can estimate the k_{2c} value using k_{2a} and k_{2b} values. Unfortunately, the k_Q value has not been measured, so that no information on k_{2c} can be obtained. Thus, a further experimental study on k_Q is required to obtain information on branching ratio of dissociation process (2c).

The nascent vibrational and rotational distributions of CH(A: v' =0–2,B: v' =0) and C_2(d: v' =0–6, C: v' =0–3, e: v' =0–6, D: v' =0–2) were determined and compared with statistical prior distributions. It was found that the reaction dynamics is not governed by statistical models but it is dominated by molecular structure of precursor state. CH(A,B) and C_2(d,C,e,D) are formed via *trans*-bent near-resonant Rydberg states converging to the first excited $\tilde{A}\,^2A_g$ state of $C_2H_2^+$. Non-linear precursor superexcited states with enlarged C≡C bond and excited CCH bending vibration led to vibrationally excited C_2* and rotationally excited CH* and C_2* fragments.

Acknowledgments

This work was supported by the Mitsubishi foundation (1996) and JSPS KAKENHI Grant number 09440201 (1997-2000).

References

1) P. Yang, N. Huang, Y. X. Leng, J. Y. Chen, R. K. Y. Fu, S. C. H. Kwok, Y. Leng, and P. K. Chu, *Biomater.*, 24, 2821 (2003).
2) P. Yang , S. C. H . Kwok, R. K. Y. Fu , Y. X. Leng, J. Wang, G. J. Wan, N. Huang, Y. Leng, P. K. Chu, *Surf. Coat. Tech.*, 177–178, 747 (2004).
3) R. S. F. Chang, D. W. Setser, and G. W. Taylor, *Chem. Phys.*, 25, 201 (1978).
4) D. H. Winicur, J. L Hardwick and S. N. Murphy, *Comb. Flame*, 53, 93 (1983).
5) D. H. Winicur, J. L Hardwick, *Chem. Phys.*, 94, 157 (1985).
6) S. Maeda, M. Yamazaki, N. Kishimoto, and K. Ohno, *J. Chem. Phys.*, 120, 781 (2004)
7) T. Horio, T. Hatamoto, S. Maeda, N. Kishimoto, and K. Ohno, *J. Chem. Phys.*, 124, 104308 (2006).
8) H. Hotop, *Adv. Mass Spectrom.*, 5, 116 (1971).
9) B. Lescop, M. B. Arfa, M.Cherid, G.L. Coz, G. Sinou, G. Fanjoux, A. Le Nadan, and F. Tuffin, *J. Electron Spectrosc. Relat. Phenom.*, 87, 51 (1997).
10) T. Ibuki and Y. Horie, *Chem. Phys. Lett.*, 196, 541 (1992).

11) T. Ibuki, Y. Horie, A. Kamiuchi, Y. Morimoto, M. C. K. Tinone, K. Tanaka, and K. Honma, *J. Chem. Phys.*, 102, 5301 (1995).
12) H. Obase, M. Tsuji, and Y. Nishimura, *Chem. Phys.*, 74, 89 (1983).
13) M. Tsuji, T. Komatsu, M. Tanaka, M. Nakamura, Y. Nishimura, and H. Obase, *Chem. Lett.*, 26, 359 (1997).
14) H. Sekiya, M. Tsuji, and Y. Nishimura, *Chem. Phys. Lett.*, 100, 494 (1983).
15) H. Obase, M. Tsuji, and Y. Nishimura, *Chem. Phys. Lett.*, 105, 214 (1983).
16) J. E. Ruett, L. S. Wang, J. E. Pollard, D. J. Trevor, Y. T. Lee, and D. A. Shirley, *J. Chem. Phys.*, 84, 3022 (1986), and references therein.
17) G. Bieri and L. Åsbrin, *J. Electron Spectrosc.*, 20, 149 (1980).
18) *NIST Chemistry WebBook*, NIST Standard Reference Database, Number 69 (2018): http://webbook.nist.gov/chemistry.
19) K. P. Huber and G. Herzberg, "*Molecular Spectra and Molecular Structure, IV. Constants of Diatomic Molecules*", Van Nostrand Reinhold, New York (1979).
20) F. C. Fehsenfeld, *J. Chem. Phys.*, 53, 2000 (1970).
21) A. Yokoyama and Y. Hatano, *Chem. Phys.*, 63, 59 (1981).
22) W. P. West, T. B. Cook, F. B. Dunning, R. D. Rundel, and R. F. Stebbings, *J. Chem. Phys.*, 63, 1237 (1975).
23) A. Aguilar, B. Brunetti, M. González, and F. Vecchiocattivi, *Chem. Phys.*, 145, 211 (1990).
24) G. Herzberg, "*Molecular Spectra and Molecular Structure, I. Spectra of Diatomic Molecules*", Van Nostrand Reinhold, Princeton (1950).
25) M. Tsuji, T. Komatsu, K. Uto, J.-I. Hayashi, and T. Tsuji, *Engineering Sciences Reports, Kyushu University*, 43, 1 (2021).
26) I. Kovács, "*Rotational Structure in the Spectra of Diatomic Molecules*", Hilger, London (1969).
27) M. Tsuji, K. Kobarai, H. Obase, H. Kouno, and Y. Nishimura, *J. Chem. Phys.*, 94, 277 (1991)
28) M. Martin, *J. Photochem. Photobiol. A: Chem.*, 66, 263 (1992).
29) J. E. Hesser and B. L. Lutz, *Astrophy. J.*, 159, 703 (1970).
30) J. Brzozowski, P. Bunker, N. Elander, and P. Erman, *Astrophys. J.*, 207, 414 (1976).
31) M. Tsuji, H. Kouno, Y. Nishimura, H. Obase, and K. Kasatani, *J. Chem. Phys.*, 95, 7317 (1991).
32) M. Tsuji, H. Kouno, H. Ujita, and Y. Nishimura, *J. Chem. Phys.*, 96, 6746 (1992).
33) H. L. Snyder, B. T. Smith, T. P. Parr, and R. M. Martin, *Chem. Phys.*, 65, 397 (1982).
34) H. Sekiya, N. Nishiyama, M. Tsuji, and Y. Nishimura, *J. Chem. Phys.*, 86, 163 (1987).
35) R. D. Levine and J. L. Kinsey, "*Atom-Molecule Collision Theory*", ed. by R. B. Bernstein, Plenum, New York (1979), p. 693.
36) R. B. Bernstein, "*Chemical Dynamics via Molecular Beam and Laser Techniques*", Oxford University Press (1982).
37) R. D. Levine, *Bull. Chem. Soc. Jpn.*, 61, 29 (1988).
38) M. Tsuji, K. Kobarai, S. Yamaguchi, H. Obase, K. Yamaguchi, and Y. Nishimura, *Chem. Phys. Lett.*, 155, 481 (1989).
39) M. Tsuji, K. Kobarai, S. Yamaguchi, and Y. Nishimura, *Chem. Phys. Lett.*, 158, 470 (1989).
40) M. Tsuji, K. Kobarai, and Y. Nishimura, *J. Chem. Phys.*, 93, 3133 (1990).
41) M. Tsuji, K. Kobarai, S. Yamaguchi, H. Obase, and Y. Nishimura, *Chem. Phys. Lett.*, 166, 485 (1990).
42) M. Tsuji, K. Kobarai, H. Kouno, H. Obase, and Y. Nishimura, *Jpn. J. Appl. Phys.*, 30, 862 (1991).

Appendix

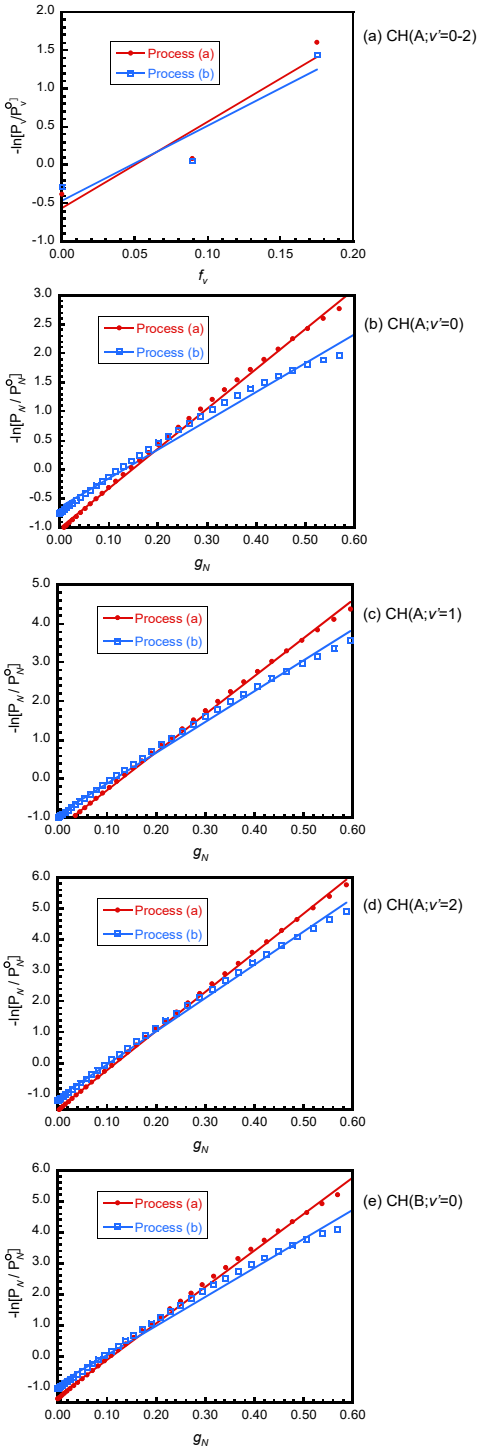

Fig. A1. (a) Vibrational surprisal plot of CH(A: v' =0–2) and (b)–(e) rotational surprisal plots of CH(A: v' =0–2) and CH(B: v'=0) in the $Ne(^3P_{0,2})/C_2H_2$ reaction.

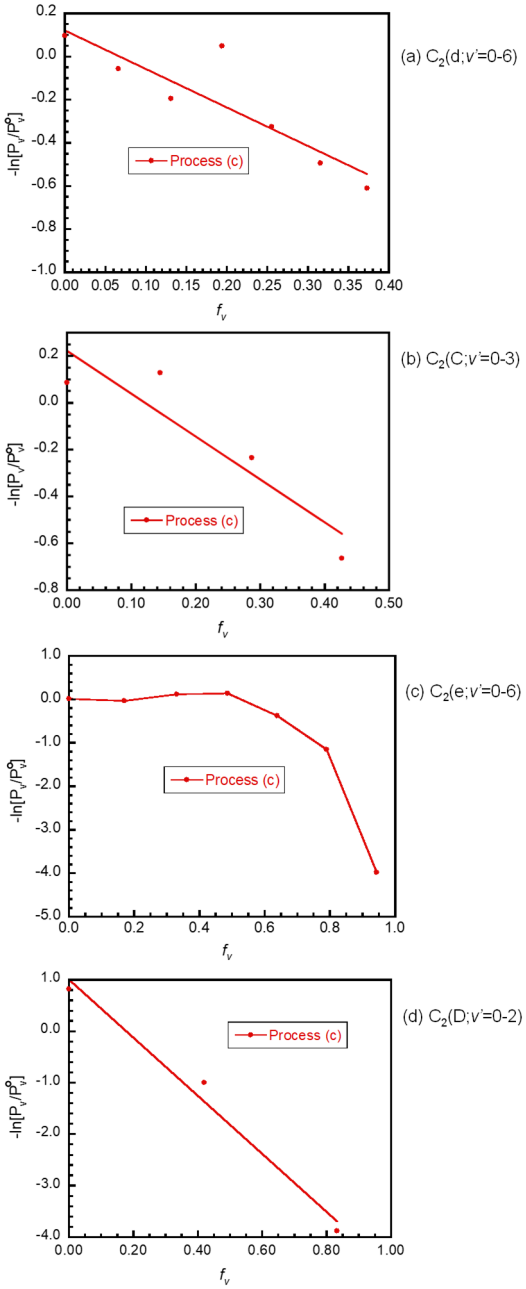

Fig. A2. (a) Vibrational surprisal plot of C_2(d: v'=0–6), C_2(C: v'=0–3), C_2(e: v'=0–6), and C_2(D: v'=0–2) in the $Ne(^3P_{0,2})/C_2H_2$ reaction.

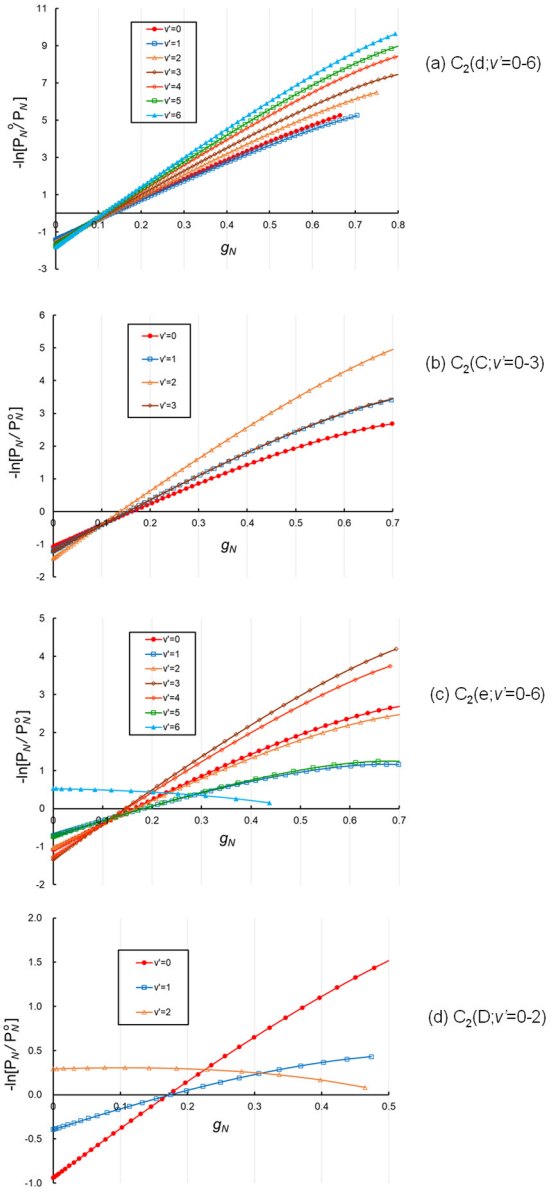

Fig. A3. (a) Rotational surprisal plot of C_2(d: v'=0–6), C_2(C: v'=0–3), C_2(e: v'=0–6), and C_2(D: v'=0–2) in the $Ne(^3P_{0,2})/C_2H_2$ reaction.

Table A1. Surprisal parameters for CH(A,B) and C_2(d,C,e,D) produced in the $Ne(^3P_{0,2})/C_2H_2$ reaction.

	Vibrational surprisal parameter		Rotational surprisal parameter	
	Two body	Three body	Two body	Three body
CH(A)	11.3	9.8		
CH(A: v'=0)			6.9	5.0
CH(A: v'=1)			9.8	7.9
CH(A: v'=2)			12.6	10.7
CH(B: v'=0)			11.8	9.4
C_2(d)		-1.8		
C_2(C)		-1,8		
C_2(e)		≈0		
C_2(D)		-5.6		
C_2(d: v'=0)				10.4
C_2(d: v'=1)				9.9
C_2(d: v'=2)				11.2
C_2(d: v'=3)				12.0
C_2(d: v'=4)				13.4
C_2(d: v'=5)				14.0
C_2(d: v'=6)				15.0
C_2(C: v'=0)				5.7
C_2(C: v'=1)				7.0
C_2(C: v'=2)				9.5
C_2(C: v'=3)				7.0
C_2(e: v'=0)				5.7
C_2(e: v'=1)				3.0
C_2(e: v'=2)				5.4
C_2(e: v'=3)				8.3
C_2(e: v'=4)				7.7
C_2(e: v'=5)				3.2
C_2(e: v'=6)				-0.8
C_2(D: v'=0)				5.0
C_2(D: v'=1)				1.9
C_2(D: v'=2)				-0.4